© 2015. Published by The Company of Biologists Ltd | The Journal of Experimental Biology (2015) 218, 824-836 doi:10.1242/jeb.106146

RESEARCH ARTICLE

Feeding in billfishes: inferring the role of the rostrum from a biomechanical standpoint

Maria L. Habegger[1,*], Mason N. Dean[2], John W. C. Dunlop[2], Gray Mullins[3], Michael Stokes[3], Daniel R. Huber[4], Daniel Winters[3] and Philip J. Motta[1]

ABSTRACT

Perhaps the most striking feature of billfishes is the extreme elongation of the premaxillary bones forming their rostra. Surprisingly, the exact role of this structure in feeding is still controversial. The goal of this study is to investigate the use of the rostrum from a functional, biomechanical and morphological standpoint to ultimately infer its possible role during feeding. Using beam theory, experimental and theoretical loading tests were performed on the rostra from two morphologically different billfish, the blue marlin (*Makaira nigricans*) and the swordfish (*Xiphias gladius*). Two loading regimes were applied (dorsoventral and lateral) to simulate possible striking behaviors. Histological samples and material properties of the rostra were obtained along their lengths to further characterize structure and mechanical performance. Intraspecific results show similar stress distributions for most regions of the rostra, suggesting that this structure may be designed to withstand continuous loadings with no particular region of stress concentration. Although material stiffness increased distally, flexural stiffness increased proximally owing to higher second moment of area. The blue marlin rostrum was stiffer and resisted considerably higher loads for both loading planes compared with that of the swordfish. However, when a continuous load along the rostrum was considered, simulating the rostrum swinging through the water, swordfish exhibited lower stress and drag during lateral loading. Our combined results suggest that the swordfish rostrum is suited for lateral swiping to incapacitate their prey, whereas the blue marlin rostrum is better suited to strike prey from a wider variety of directions.

KEY WORDS: Billfish feeding, Biomechanics, Functional morphology

INTRODUCTION

The billfishes (marlins, spearfishes, sailfishes and swordfish) are large and fast pelagic predators characterized by the extreme elongation of their upper jaw bones to form an elongated rostrum, or bill (Nakamura, 1985; Davie, 1990; Fierstine, 1990; Fierstine and Voigt, 1996). Surprisingly, the function of this structure is still controversial (Nakamura, 1983; Frazier et al., 1994). The rostrum has been hypothesized to improve hydrodynamics by reducing drag (Wisner, 1958; Ovchinnikov, 1970; Aleyev, 1977; but see Sagong et al., 2013), to be used for defense (as evidenced by rostral fragments found embedded in large predators; Fierstine, 1997; Fierstine et al., 1997) and to be used to strike, immobilize or dismember prey before ingestion, thereby facilitating feeding (Gudger, 1940; Talbot and Penrith, 1964; Scott and Tibbo, 1968). Although it is certainly possible that the elongated rostrum may have been selected for multiple roles, substantial evidence from stomach contents and recent field observations strongly support the latter feeding-related hypothesis (Scott and Tibbo, 1968; Stillwell and Kohler, 1985; Frazier et al., 1994; Shimose et al., 2007; Domenici et al., 2014).

The geometries and relative sizes of the rostra of different billfish species are in some cases strikingly different, suggesting that the use of the rostrum in feeding is species specific. The rostrum of swordfish (the only species within the Xiphiidae), which can exceed 50% of body length, is wide, distally tapered and dorsoventrally flattened with a lenticular cross-section, having sharp edges and lacking teeth (Gregory and Conrad, 1937; Gudger, 1940; Poplin et al., 1976; Nakamura, 1983; Fierstine, 1990; Fierstine and Voigt, 1996; Nohara et al., 2003). Conversely, in istiophorids (marlins, spearfishes and sailfishes), the rostrum is more circular in cross-section, has no sharp edges, and is surrounded by small villiform teeth. The length of the rostrum varies among species but is proportionally shorter than in swordfishes, being approximately 24% of body length in blue marlin (Gudger, 1940; Nakamura, 1983). These structural differences between swordfish and marlin are indeed reflected in anecdotal accounts of feeding events, where swordfish are suggested to slash their prey with only lateral movements of the rostrum (Scott and Tibbo, 1968; McGowan, 1988) and istiophorids stun and/or spear their prey, thereby using a wider range of rostral movements (Talbot and Penrith, 1964; Fierstine, 1997; Fierstine et al., 1997; Shimose et al., 2007). Correlations of these differences in rostral form and behavior between species, and their mechanical implications at the tissue level have, however, been nearly impossible to study because of the logistical issues associated with the study of large, fast, pelagic predators such as billfishes (but see Domenici et al., 2014).

Biomechanical approaches offer feasible ways to investigate the potentially differing roles of the rostrum in the various billfish species, enabling quantification of mechanical performance and facilitating the inference of behavior from morphology. The utility of these approaches has been demonstrated for experimentally intractable taxa, via investigations of feeding mechanics in white sharks, bull sharks and rorqual whales (Wroe et al., 2008; Field et al., 2011; Habegger et al., 2012). Significant advances in biomechanical studies have been accomplished through the utilization of beam theory, an engineering approach that describes the mechanical behavior of a beam under loading. This approach is applicable because many biological structures can be treated as beams (e.g. trees, echinoderms, vertebral columns; Koehl, 1977; Baumiller, 1993; Ennos, 1993; Huber et al., 2013), and beam theory also facilitates better comprehension of form and function

[1]Department of Integrative Biology, University of South Florida, 4202 E. Fowler Ave, Tampa, FL 33613, USA. [2]Department of Biomaterials, Max Planck Institute of Colloids & Interfaces, Am Muehlenberg 1, Potsdam 14476, Germany. [3]Department of Civil and Environmental Engineering, University of South Florida, 4202 E. Fowler Ave, Tampa, FL 33613, USA. [4]Department of Biology, University of Tampa, 401 W. Kennedy Blvd, Tampa, FL 33606, USA.

*Author for correspondence (mhabegge@mail.usf.edu)

Received 13 April 2014; Accepted 8 January 2015

The Journal of Experimental Biology

The Journal of Experimental Biology (2015) 218, 824-836 doi:10.1242/jeb.106146

relationships by teasing apart factors that contribute to a biological beam's performance under loading. A beam's resistance to bending is given by the flexural stiffness *EI*, which is a function of both its material properties (via Young's modulus, *E*) and its geometry (via second moment of area, *I*) (Koehl, 1976, 1977; Wainwright et al., 1976; Biewener and Full, 1992). Analyses of a structure's cross-sectional geometry and the response of its material to load (e.g. the force per unit area, or stress, σ, that builds in a material under load in response to deformation, or strain, ε) can therefore provide an understanding of the overall structure's mechanical capabilities and limits, with stress distributions and yield behavior pointing to performance boundaries, all of which can offer clues to loading regimes likely to be experienced *in vivo*. Because *EI* accounts for both material and structural properties, it is a useful metric for characterizing mechanical function in comparative studies, particularly when linking organismal function with evolutionary and ecological pressures (Koehl, 1976, 1977; Macleod, 1980; Etnier, 2003). Flexural stiffness has been shown to correlate with loading regime and direction for a range of biological body support systems, from the limb skeletons of batoids and dogs, to the jaws of whales and pelicans, to the exoskeletons of crabs (Kemp et al., 2005; Taylor et al., 2007; Field et al., 2011; Macesic and Summers, 2012); these taxonomic comparisons also illustrate that higher levels of bending resistance can be attained evolutionarily by increases in either *E* or *I*, or in both.

The goal of this study is to use biomechanical models and material testing to infer the possible biological role(s) of the rostrum in two billfish species with differing rostrum morphologies, the blue marlin (*Makaira nigricans* Lacepede 1802) and the swordfish (*Xiphias gladius* Linnaeus 1758). Utilizing beam theory as our primary model, we estimate several biomechanical variables and describe the material properties and geometric attributes of the rostrum along its length in order to acquire a better understanding of its function and mechanical capabilities. Inferences of the putative feeding behaviors of these two apex predators are then made based on these analyses, paying special attention to suggestions of how mechanical and growth demands may be balanced for these biological cantilevers. Since failure or large deflections could be detrimental during feeding we hypothesize that stress will be equally distributed along the length of the rostrum, preventing any localized region of higher stress ('weak spots') that could lead to failure during feeding. Correspondingly, we expect flexural stiffness to be uniform along the length of the rostrum and sufficiently large to avoid appreciable deflections while striking prey. Based on previous descriptions of cross-sectional geometry, we expect that the swordfish rostrum will be better suited for lateral striking of prey, whereas that of the blue marlin will be suited for a larger range of motions.

RESULTS

Histology

The rostra of both species are composed of similar tissue types that appear to be arranged in similar patterns along the length of the rostra (Figs 1 and 2). Three main tissues were observed: acellular bone (a bone lacking osteocytes, Cohen et al., 2012), adipose tissue, and hyaline cartilage, with proportions of the tissues changing in distinct ways from tip to base. The primary component of distal cross-sections (Fig. 1A–D and Fig. 2A–D) was acellular bone. Moving proximally towards the base of the rostrum, adipose tissue and hyaline cartilage become more dominant, particularly in area 4, where they comprise most of the center of the cross-section (Fig. 1E,F and Fig. 2E,F) and acellular bone is relegated to the periphery. Although the majority of the adipose tissue was found in area 4, this tissue was also observed intermittently in smaller quantities within canals present throughout the acellular bone of the rostrum.

Geometric analysis

Swordfish and blue marlin exhibited diagnostic differences for most of the variables in our CT-scan-based analysis of cross-sectional geometry, indicating that the observed species-specific morphologies have mechanical consequences. Second moment of area (*I*, a descriptor of the cross-sectional distribution of material in the direction of loading and a proxy for bending resistance) increased proximally in both species and in both principle loading directions, particularly at ∼75–80% bill length (BL), where the rostrum begins to merge with the head region. However, the ratio of *I* for loading in the dorsoventral and lateral directions (I_{maj}/I_{min}) differed considerably between species, as a function of the dissimilar cross-sectional shapes of the rostra. Swordfish rostra are extremely asymmetric in morphology and in the contribution of rostrum shape to bending resistance, with *I* in lateral bending ∼10–16 times greater than that for dorsoventral bending. This ratio is greatest distally and decreases proximally as the rostrum deepens closer to the head (Fig. 3A). In blue marlin, *I* was only slightly greater for loading in the lateral direction, and the ratio of I_{maj}/I_{min} was fairly constant along the length of the rostrum (∼2–3), indicating a more uniform distribution of material and isotropic bending resistance (Fig. 3B; Table 1).

In proximal regions of the rostrum, bone forms only a thin peripheral layer but is arranged far from the neutral axis, resulting in a high *I* for a comparatively small amount of bone tissue. This is reflected in the abrupt proximal (∼75–80% BL) decrease in the proportion of mineralized tissue in each cross-section (Fig. 3C,D), as well as in our histological data, which show a proximal decrease in bone and increase in adipose tissue and cartilage (Figs 1,2). Whereas in blue marlin the proportion of mineralized tissue in cross-sections is approximately 100% in distal sections (<80% BL), representing a solid bony rostrum, in swordfish the proportion of mineralized tissue shows jagged oscillation distally, reflecting the periodic bony chambers (Fierstine, 2006) within the distal rostrum (Fig. 3C). Both species show a proximal-to-distal increase in the mean relative bone mineral density of the rostra, whereas the pattern of decrease in swordfish is more gradual, and that of blue marlin is consistent until approximately 70% BL and then decreases more sharply (Fig. 3C,D).

Bending experiments in a material testing system (MTS)

Stresses along the rostrum were calculated as a function of rostral geometry and load during bending experiments where rostra tips were displaced ±1 cm. Although the magnitude of stresses in the rostra of the two species were considerably different, with blue marlin stresses being two to four times higher, both species showed an approximately similar distal-to-proximal trend of slight increase in stress from area 1 to 2 and then a gradual decrease to area 4. During lateral loading, the average maximum stress distribution did not vary much along the swordfish rostrum, ranging from 1.4 to 1.6 N mm^{-2} (areas 1–4, respectively). During dorsoventral loading, the stress distribution was higher along the rostrum ranging from 2.1 to 1.3 N mm^{-2} (areas 1-4, respectively, Fig. 4A, supplementary material Table S1). For the blue marlin, the average maximum stress distribution during lateral loading ranged from 7.8 to 3.9 N mm^{-2} (areas 1–4, respectively) with stress in the three most distal areas being considerably greater than that in the most proximal section (area 4). Similarly, during dorsoventral loading, the stress distribution in the three distal areas ranged from 8.7 to 9.2 N mm^{-2}, and area 4 decreased to 4.9 N mm^{-2} (Fig. 4B, supplementary material Table S1).

The Journal of Experimental Biology (2015) 218, 824-836 doi:10.1242/jeb.106146

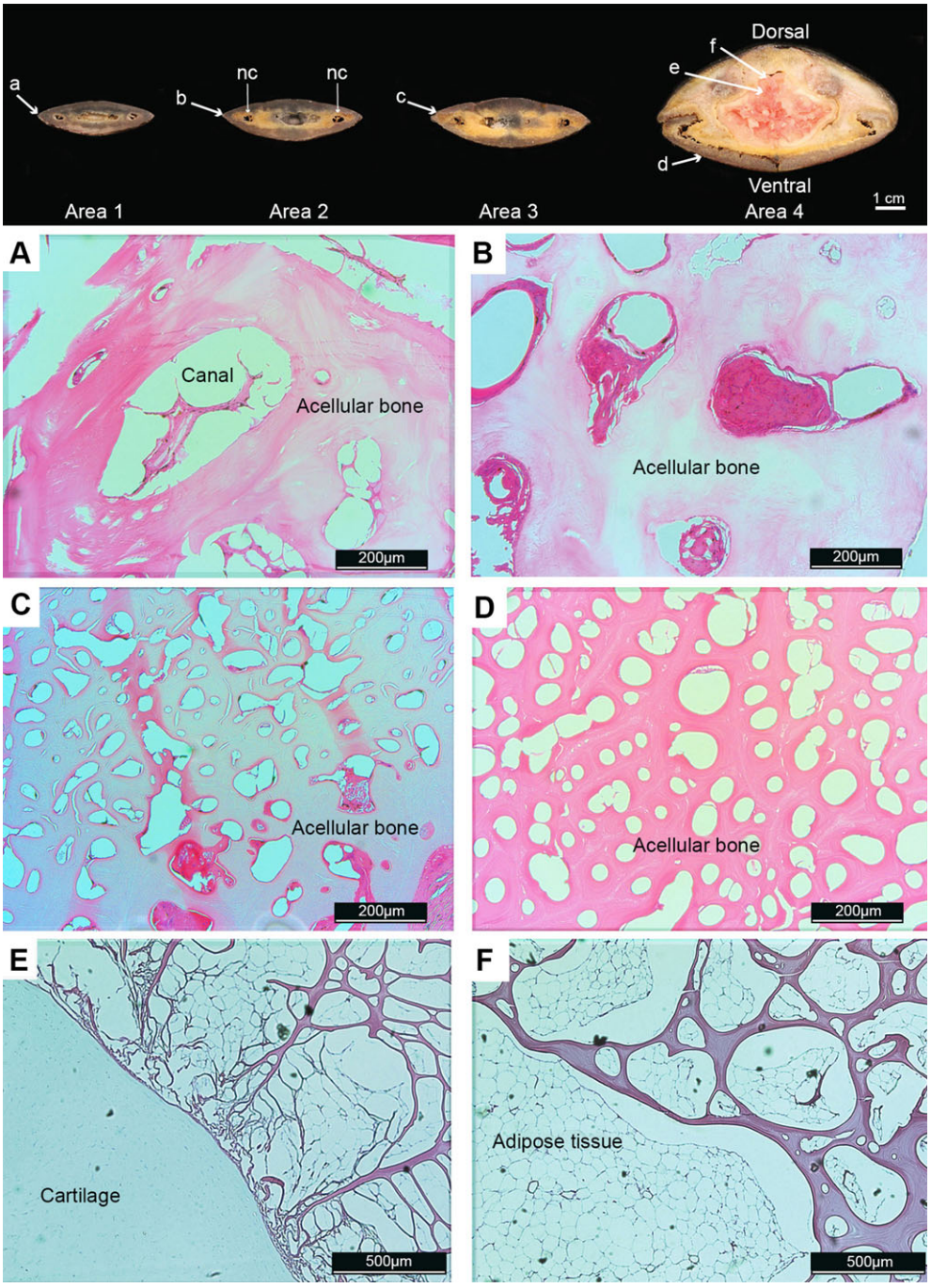

Fig. 1. Histological analysis performed along four regions of the rostrum of a swordfish. Top image from left to right shows representative cross-sections from areas 1 to 4. Arrows indicate locations of sampled regions shown in A–F. (A–D) Acellular bone is present in all areas. (E,F) Different tissues found on area 4 including cartilage and adipose tissue. Cross-section orientation: dorsal on top, ventral on bottom. Upper surface of cross-section is the dorsal portion of the rostrum; nc, nutrient canals.

In the swordfish, Young's modulus, E, decreased proximally from 12.2 to 5.3 GPa when calculated in lateral loading (areas 1–4, respectively) and from 12.9 to 3.1 GPa when calculated in dorsoventral loading (Fig. 4C, supplementary material Table S1). Although similar trends in E were observed for the blue marlin, values tended to be larger, ranging from 14.5 to 3.5 GPa in lateral loading and from 16.4 to 5.7 GPa in dorsoventral loading (Fig. 4D, supplementary material Table S1).

Flexural stiffness, which accounts for both material and geometric contributions to bending resistance, increased proximally in the swordfish during lateral (3.7×10^5 to 9.6×10^5 GPa mm^4) and dorsoventral loading (2.9×10^4 to 1.2×10^5 GPa mm^4) (Fig. 4E). Flexural stiffness also increased proximally in the blue marlin, although values between the two loading planes were more similar than those of the swordfish, especially for the distal half of the rostrum. During lateral loading, EI ranged from 4.2×10^5 to 2.0×10^6 GPa mm^4 and dorsoventrally from 2.4×10^5 to 1.3×10^6 GPa mm^4 (Fig. 4F). (For the full range of values, see supplementary material Table S1.)

It took considerably larger loads to displace the blue marlin rostrum the same fixed distance (±1 cm) as that of the swordfish (maximum loads applied to the blue marlin rostrum were 173.0 N and 123.9 N compared with the swordfish 19.3 N and 7.1 N, lateral and dorsoventral loading, respectively). Therefore, rather than comparing stresses resulting from the maximum loads applied to rostra of both species, we determined the largest moment value during the swordfish experiments, and then for each strain gauge, determined the corresponding stresses resulting from a similar

The Journal of Experimental Biology (2015) 218, 824-836 doi:10.1242/jeb.106146

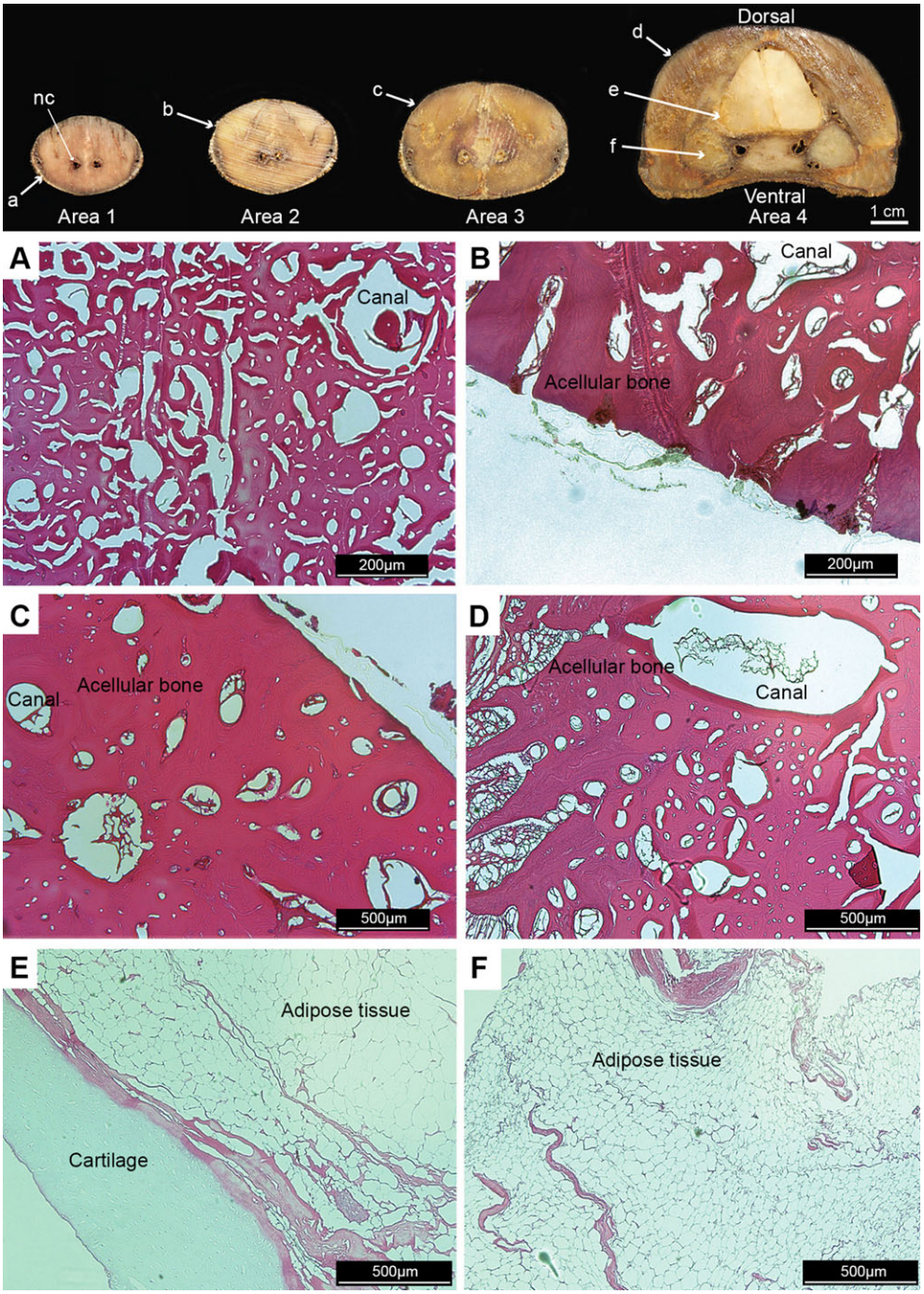

Fig. 2. Histological analysis performed along four regions of the rostrum of a blue marlin. Top image from left to right shows representative cross-sections from areas 1 to 4. Arrows indicate the locations of sampled regions shown in A–F. (A–D) Acellular bone is present in all areas (white areas around the edge of the rostrum in B and C show no tissue). (E,F) Different tissues found on area 4, such as cartilage and adipose tissue. Cross-section orientation: dorsal on top, ventral on bottom. Upper surface of cross-section is the dorsal portion of the rostrum; nc, nutrient canals.

moment value in both blue marlin specimens. This 'standardized' stress allowed us to illustrate the difference in the tissue stress responses to the same moment, as opposed to the responses to the same maximum displacement. The use of the swordfish maximum moment as a reference value for both species was preferred over load standardizations (standardizing the values to similar loads for each species) to account for small differences in the position of the strain gauges between species because bending moment calculations take into account both load and distance from load. Results from standardized moments showed similar stress values for both species during lateral loading with the exception of area 4 for blue marlin, which was considerably lower. However, during dorsoventral loading, swordfish rostra showed almost three times greater stresses (Table 2, Fig. 5A,B).

Biological loading scenarios: point loading and hydrodynamic loading

For a hypothetical point loading scenario, swordfish had higher stress values along the rostrum in both loading planes compared with blue marlin (Fig. 6A). Stresses calculated for the swordfish rostrum during dorsoventral loading were considerably larger than those for lateral loading, diminishing towards the base (Fig. 6A). Stress values for blue marlin were lower and very similar for both loading planes. Simulations of hydrodynamic loading during head swinging indicated that swordfish experience the highest maximum stress and drag during dorsoventral loading and lowest maximum stress and drag during lateral loading, with blue marlin values being intermediate for both variables in both loading directions (Fig. 6B,C).

The Journal of Experimental Biology (2015) 218, 824-836 doi:10.1242/jeb.106146

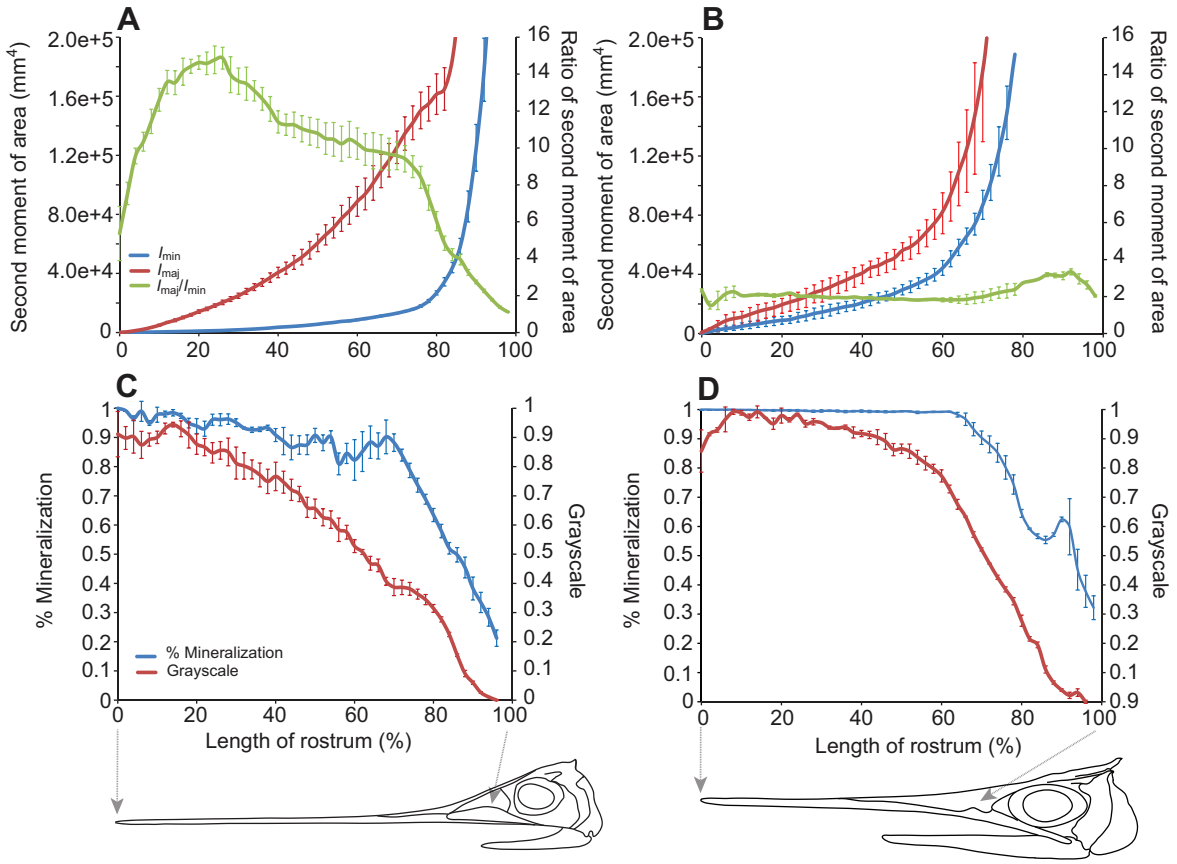

Fig. 3. Geometric analysis along the length of the rostrum of swordfish and blue marlin. Rostrum length is indicated as a percentage; 0%=distal tip, 100% =proximal base. Swordfish (left column, mean±s.e., n=4) and blue marlin (right column, mean±s.e., n=2). (A,B) Second moment of area (I, mm^4) about the dorsoventral plane (I_{min}), the lateral plane (I_{maj}) and the ratio between second moments of area (I_{maj}/I_{min}). (C,D) Percentage cross-sectional area occupied by bone tissue (% mineralization) and the relative bone tissue grayscale values (a proxy for bone mineral density, calculated relative to each CT scan's maximum).

DISCUSSION

Our data suggest that the morphological differences observed between swordfish and blue marlin rostra have performance implications, and that these morphological and mechanical differences may be consistent with different feeding behaviors. Considering the possible role of the rostrum during feeding, the blue marlin rostrum is built like a short, solid javelin with cross-sectional anatomy suggesting multi-axial use; in contrast, the swordfish rostrum appears suited for use as a light-weight, low drag, uniaxial weapon.

Despite the cross-sectional shape differences between the two species, our data show several material and structural commonalities between blue marlin and swordfish rostra, providing strong evidence that common evolutionary pressures (e.g. growth, use in feeding) may have shaped rostral anatomy in both species. In general, both rostra show opposing trends in I and E, with the former increasing rapidly proximally, but the latter increasing distally (Fig. 3, Fig. 4C,D). The decrease in E proximally means that the increase in EI must solely result from disproportionate changes in I. The distribution of grayscale intensity in rostrum CT scans suggests that bone mineral density increases distally in the rostrum in both species (Fig. 3C,D), perhaps explaining the observed stiffness gradient, because E and mineral density are positively associated in a variety of mineralized tissues (Currey, 2004; Horton and Summers, 2009; Magwene and Socha, 2013).

Stress values in the tissue resulting from the bending experiments were shown to be approximately similar among the distal regions (areas 1–3) for both species (Fig. 4A,B). A strategy to keep stress constant along the length of a cantilever beam is to increase the cross-sectional area towards the fixed end, compensating for the increase in bending moment (Currey, 1984). Billfish rostral cross-sectional area and I increase proximally (Figs 1–3), probably explaining the consistent stresses in the distal regions. Stress values tended to be comparatively low in area 4, achievable because of the comparatively large I values at the base (>60% bill length). This increase in I is a function of the change in geometry and the large cross-sectional areas in proximal regions, but also the peripheral arrangement of bone in this area. This arrangement allows for a high I without necessitating increased weight, because the core of the base of the rostrum is filled with low density materials (adipose

Table 1. Second moment of area obtained from MATLAB geometrical analysis along the rostrum of two billfish species: swordfish (*X. gladius*) and blue marlin (*M. nigricans*)

	Area 1	Area 2	Area 3	Area 4
SWF_{LAT}	27,241	56,466	104,200	168,425
SWF_{DV}	2243	5537	10,939	37,397
BM_{LAT}	29,797	48,747	104,991	603,445
BM_{DV}	15,139	25,917	57,228	224,365

Second moment of area (mm^4) at four regions along the rostrum (area 1 to area 4) for swordfish (SWF) and blue marlin (BM) during lateral (LAT) and dorsoventral (DV) bending.

The Journal of Experimental Biology (2015) 218, 824-836 doi:10.1242/jeb.106146

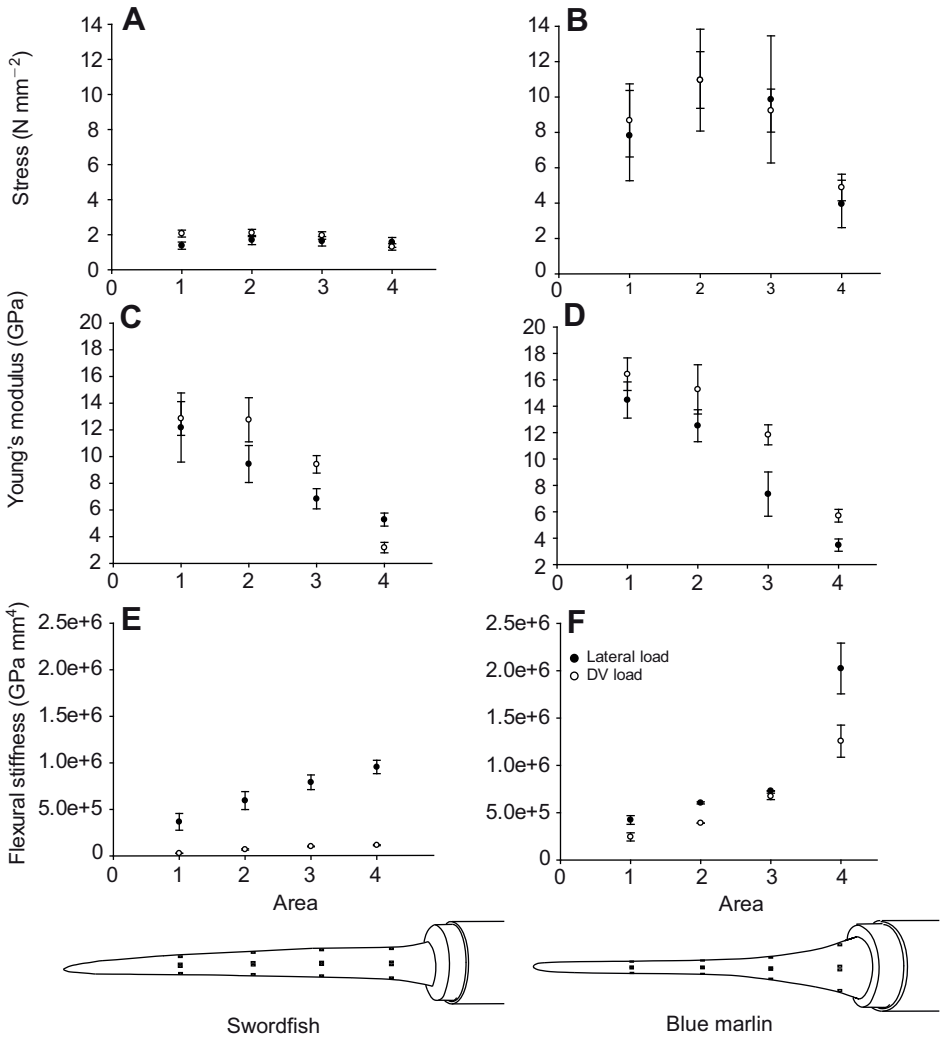

Fig. 4. Intraspecific results from bending experiments in two loading planes. Values are mean±s.e. for swordfish (left) and blue marlin (right). (A,B) Stress distribution along the rostrum (N mm^{-2}). (C,D) Young's modulus (GPa). (E,F) Flexural stiffness (GPa mm^4). Black and white circles denote different loading orientations; DV, dorsoventral.

tissue and cartilage) that are lighter than a comparable rostrum of solid bone (Figs 1 and 2, area 4). Biological structures that have a similar conformation (solid exterior and a softer, light-weight interior) such as the toucan beak, porcupine quills and feather shafts (Bonser, 2001; Seki, et al., 2005; Meyers et al., 2013) have been suggested to not only increase I in a structure but also to decrease the probability of local buckling by dissipating fracture energy and preventing the collapse of the thin cortical walls, while also minimizing weight (Ma et al., 2008; Meyers et al., 2013). Furthermore, Gudger (1940) proposed this filling in billfishes may also act as shock absorber, dampening vibrations during striking of prey.

The ecological implications of the distal increase in material stiffness may be associated with feeding, because this change minimizes deflection of the distal portion of the rostrum and provides a hard surface for striking prey. Billfish rostra are subject to periodic loadings over long periods of time, which may result in fatigue damage and favor the formation of microcracks in this stiffer area, as in bone and nacre (Currey, 1984). Similar gradients of stiffness have been reported in other biological structures including bird feathers (Macleod, 1980; Bonser and Purslow, 1995), squid beaks (Miserez et al., 2008) and spider fangs (Politi et al., 2012); the latter two systems also acting as predatory weapons, similar to billfish rostra. In addition, the higher incidence of remodeled bone morphology in the distal region of the rostrum suggest that the tissue is under regular loading and therefore more prone to damage and consequently, remodeling (Atkins et al., 2014). Distal stiffening of rostral material could also counteract structural tapering relating to hydrodynamic demands. Previous work has shown that the drag experienced during lateral swiping of the elongate rostrum in alligators is proportional to the height of the jaws (McHenry et al., 2006). Minimizing element height (via distal tapering) may reduce drag in billfish rostra; however, it also comes at the cost of potentially reducing cross-sectional area and resistance to bending (McHenry et al., 2006); distal stiffening of the rostrum may ultimately be a strategy for maintaining adequate flexural stiffness in areas where I is selected to be comparatively low for hydrodynamic reasons. Additionally, since the bow wave generated by a predator can be detected by prey (Visser, 2001), the relatively smooth and

Table 2. Standardized values of stress obtained from bending experiments in the blue marlin and swordfish

	Area 1	Area 2	Area 3	Area 4
SWF_{LAT}	1.4±0.2	1.7±0.3	1.6±0.3	1.6±0.3
SWF_{DV}	2.1±0.2	2.1±0.2	2.0±0.2	1.3±0.2
BM_{LAT}	1.3±0.2	1.9±0.2	1.7±0.3	0.7±0.3
BM_{DV}	0.7±0.1	1.0±0.1	0.8±0.0	0.4±0.0

Standardized stress values (N mm^{-2}) in blue marlin (BM) along the rostrum (mean±s.e. areas 1 to 4, respectively) during lateral (LAT) and dorsoventral (DV) bending.

The Journal of Experimental Biology (2015) 218, 824-836 doi:10.1242/jeb.106146

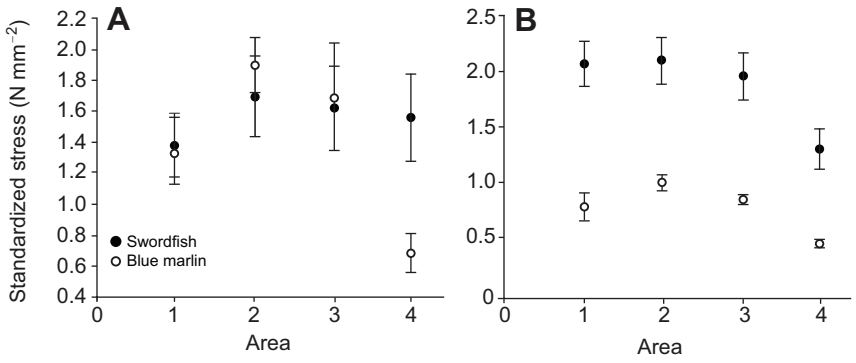

Fig. 5. Interspecific comparisons of standardized stress (N mm^{-2}) from bending experiment in two loading planes. (A) Lateral plane and (B) dorsoventral plane (mean±s.e.). Standardizations were performed in blue marlin (white circles) whereas swordfish values (black circles) were not modified.

elongated rostrum of billfishes may reduce water disturbance, thereby delaying detection of approaching billfish by prey, as suggested for other vertebrates with long jaws including water snakes and alligators (Alfaro, 2002; McHenry et al., 2006).

Generalized patterns of stress, material stiffness, second moment of area, and flexural stiffness in rostra of both billfish seem to follow a common pattern that may aid in overcoming conflicting demands imposed by the rostrum's function and shape. Evidence from the histology and mineral density gradient of the rostrum found in this study, in addition to that in an ongoing investigation of billfish tissue morphology (Atkins et al., 2014), indicate that distal regions of the billfish rostrum are less porous, more mineral dense and more remodeled. This suggests that distal areas may contain older tissue than basal regions and therefore that the rostrum in billfishes may grow from its base by 'pushing' older material distally (although rostrum development is not fully understood and other factors such as mechanical demands may play a role in its development). We have shown that basal regions of the rostrum (i.e. suggested growth zones) are prone to less stress and, because of the proximal increase in I, EI was also increased. The lower values of stress at the base of rostrum also coincide with a region of multiple sutures, where multiple cranial bones converge and where the rostrum connects to the rest of the head (Fig. 7). Sutures have been found to influence patterns of stress and strain by resisting or allowing deformations depending on load orientation and/or magnitude (Rafferty et al., 2003; Markey et al., 2006; Krauss et al., 2009) but can also act as bone deposition sites in mammals (Opperman, 2000; Sun et al., 2004) and so may provide free surfaces for growth and bone deposition in billfish rostra. All of these factors may decrease the likelihood of failure at this region, preventing the compromise of vital organs such as the nares, and also preventing damage to a region of higher vascularization and growth. Coincidentally, rostra in several different billfish species have been more often documented to show breaks in their distal halves (Frazier et al., 1994; Fierstine and Crimmen, 1996; Fierstine et al., 1997).

Although broad structural similarities clearly exist between rostra of these species, their morphological differences revealed mechanical disparities that suggest different feeding behaviors. While I was approximately equal for both species during lateral loading (Fig. 3A,B), the blue marlin rostrum showed higher I during dorsoventral loading and greater equivalence of bending resistance between lateral and dorsoventral loading (I_{maj}/I_{min}~1.0) as a result of its almost circular cross-section, compared with the swordfish (I_{maj}/I_{min}>8.0) (Fig. 3A,B). Additionally, blue marlin rostra showed E values higher than those for swordfish for most of the regions along the rostrum (Fig. 4C,D) and E varied with respect to loading regime in swordfish, suggesting material heterogeneity in this species. Overall, stiffness values calculated from distal strain gauge data (area 1, 12.9 GPa swordfish and 16.4 GPa blue marlin) agree with those determined in a different study for five billfish species (including those studied here) using material testing techniques (E ranged between 12 and 20 GPa; Atkins et al., 2014) but also exceed the values found in other acellular boned fishes, such as great sculpin, *Myoxocephalus polyacanthocephalus* (6.48 GPa; Horton and Summers, 2009) and tilapia *Oreochromis aureus* (7.20 GPa; Cohen et al., 2012) as well as those with cellular bone found in the common carp *Cyprinus carpio* (8.51 GPa; Cohen et al., 2012). Moreover, values of stiffness in billfish are not only shown to be higher than most values reported for other fish, but also to be closer to values reported for mammals (Atkins et al., 2014).

Mechanical demands associated with feeding may not be the only factors dictating shape differences between species. Drag forces, for example, are influenced by a structure's shape, surface characteristics, speed of movement and the surrounding fluid's density and viscosity (Vogel, 2003), and therefore drag forces acting on the rostra can conceivably influence feeding. Our results from modeled biological loading scenarios indicate that drag force and stress during dorsoventral loading are greater in swordfish than blue marlin. Swordfish rostra, however, would exhibit the lowest drag force during lateral loading (Fig. 6C) because of the depressed lenticular form of the rostrum. Consequently, swordfish may be limited in the extent to which they can use dorsoventral striking, which incurs 40-times higher drag forces than lateral striking (Fig. 6C). Interestingly, this support for differences in rostrum motion during striking are also suggested by differences in vertebral morphology between the two species. The vertebral column of the blue marlin is reinforced with zygapophyses, which provide reinforcement and stability but decrease flexibility (Hebrank et al., 1990). In contrast, the lack of zygapophyses in swordfish may allow extensive lateral flexibility of their body, because Hebrank et al. (1990) found that the flexibility of the blue marlin vertebral column increased when the zygapophyses were removed. The potentially greater lateral flexibility of the swordfish body may be related to the dorsoventral depression of the rostrum and its reduced hydrodynamic drag in the horizontal plane, facilitating low-resistance, lateral swiping at its prey.

Patterns of σ, E, I, EI and theoretical drag calculations suggest that blue marlin may have a rostrum better suited to strike its prey in a wider range of motions, similar to the multi-plane striking behavior observed during feeding in sailfish (Domenici et al., 2014), a species with a rostrum similar in shape to that of the blue marlin. Rod-like structures are suited to withstand loading in multiple directions, whereas elliptical cross-sectional beams, such as the swordfish rostrum, are better designed to withstand loading in a single plane (Etnier and Vogel, 2000; Currey, 2002). Injuries to prey provide insight into billfish feeding behavior (Scott and Tibbo, 1968; Nakamura, 1985; Stillwell and Kohler, 1985). Prey fishes in the stomach contents of blue marlin showing lacerations to the

The Journal of Experimental Biology (2015) 218, 824-836 doi:10.1242/jeb.106146

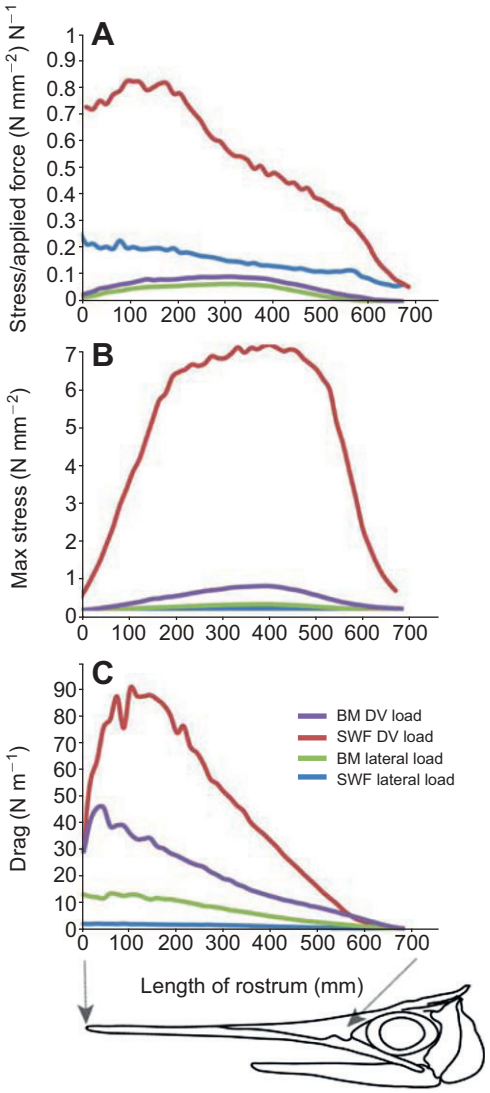

Fig. 6. Comparisons of localized and continuous loads among species and loading orientations. (A) Stress applied at a localized point. (B) Load continuously applied along the rostrum. (C) Drag forces along the rostrum. Each color represents a species with a particular loading plane, blue lines are swordfish loaded laterally, red lines swordfish loaded dorsoventrally, green lines blue marlin loaded laterally and purple lines blue marlin loaded dorsoventrally. Rostrum length is shown from 0 (most distal part) to 700 (most proximal portion).

dorsal, ventral and caudal body regions (Shimose et al., 2007) and images of sailfish prey bearing injury on differing regions of the body (Fig. 8A) support our theory of multi-directional striking in istiophorids. In contrast, gut contents of swordfish showed prey being severed, which may be due to the lateral swiping of the sharp, lenticular rostrum (Goode, 1883; Stillwell and Kohler, 1985) (Fig. 8B).

In conclusion, blue marlin rostra are stiffer and better suited to strike prey in multiple planes, whereas swordfish rostra seem to be highly specialized for lateral striking as a result of the arrangement of skeletal material in a way that maximizes lateral bending resistance while decreasing drag. However, despite the differences found between these species, there are still many variables converging into similar patterns that may explain how to build an efficient biological beam that can act as a weapon in multiple ways. Whether this structure evolved as an adaptation for feeding remains uncertain, but its design, tissue architecture, and material properties favor its role in prey capture.

MATERIALS AND METHODS

Tissue preparation

Four swordfish (*Xiphias gladius*) and two blue marlin heads (*Makaira nigricans*) (Table 3) with intact rostra were obtained from fishing tournaments in the Gulf of Mexico, USA. Heads were transported to the University of South Florida and frozen with the rostrum wrapped in plastic to reduce dehydration. After being thawed, all heads were CT scanned with a 64-slice Aquilon Toshiba scanner (Toshiba American Medical Systems Inc., Tustin, CA, USA) with slice thickness ranging from 0.75 to 1.0 mm (image size, 512×512 pixels; pixel size, 0.625 mm). After scans were completed, samples were wrapped in plastic bags and kept frozen until material testing. Whole-skull scans were rendered for figure purposes using Mimics software (Materialise HQ, Belgium). The use of all tissue samples was approved under the University of South Florida Institutional Animal Care and Use Committee, IACUC protocol number T 3884.

Histology

In order to investigate the tissues comprising the rostra, transverse sections were prepared for both swordfish (n=1) and blue marlin (n=1) at four regions along each rostrum, mirroring the locations of strain gauge placement (see below). Four transverse sections (areas 1–4, distal to proximal) of approximately 0.5 cm thickness were cut from one representative rostrum of each species. Transverse sections were preserved in 10% buffered formalin followed by decalcification in formic acid (50% HCOOH, 50% H_2O) sodium citrate (500 g $NaH_2C_6H_5O_7$, 2500 ml H_2O). Sections of 4 µm were made with a Bioacut microtome (Leica/Reichert Jung model 2030, Wetzlar, Germany) and stained using hematoxylin and eosin. Samples were observed under compound microscope (Leica CTR 6500 Wetzlar, Germany). Pictures were taken at two magnifications, ×50 and ×100, with a digital camera (Leica DFC 420c Wetzlar, Germany). Although this tissue had been subjected to previous freeze–thaw cycles, which may compromise bone tissue and cellular ultrastructure (e.g. nuclei and osteocytes; Andrade et al., 2008), these changes are irrelevant for the scale of our observations and osteocytes are lacking from the bone of these species.

Geometric analysis

In order to understand geometric and structural contributions to the mechanical performance of billfish rostra, we applied beam theory analyses to transverse sections of the rostra of four swordfish and two blue marlin (Table 3) using a custom MATLAB script described below. Our analyses were restricted to the contribution of hard tissue (bone) because CT scanning captures only bone structure accurately and bone occupies the majority of the rostra.

Rostral bone was isolated within each dataset using the Segmentation Editor in Amira (Mercury Computer Systems, Berlin, Germany) by first digitally isolating the rostrum (by cropping out all tissue caudal to the nares).

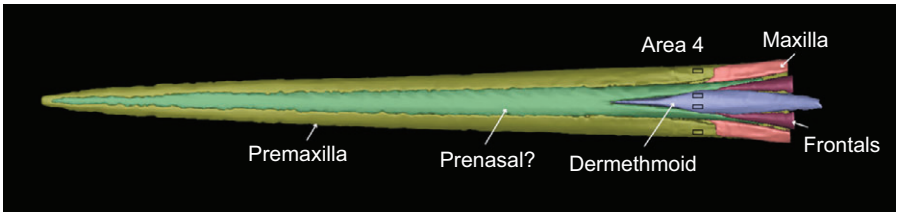

Fig. 7. CT scan reconstruction of a swordfish rostrum. Bones are individually labeled and colored; the locations of the strain gauges are marked in area 4 to illustrate their arrangement in this highly sutured area on the proximal portion of the rostrum. Bone nomenclature follows Fierstine and Voigt (1996); however, the prenasal bone is still controversial for this species and is indicated with a question mark (see Fierstine, 1990).

The Journal of Experimental Biology (2015) 218, 824-836 doi:10.1242/jeb.106146

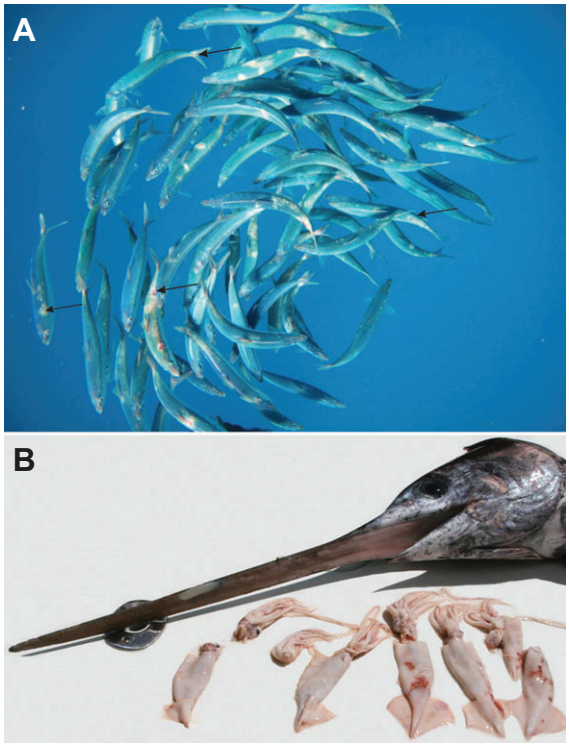

Fig. 8. Prey injuries evidencing the use of the rostrum during feeding. (A) Injuries in prey items after a sailfish (*Istiophorus albicans*) feeding event in Isla Mujeres, Mexico. Arrows denote possible multiplane points of impact from the rostrum (R. de la Parra, personal communication). (B) Decapitated squid from stomach contents of a swordfish suggesting that lateral slashing is used during feeding behavior (E. Walker, personal communication). Because in both cases direct feeding events were not documented, other types of feeding behavior may be equally viable.

The rostrum includes a range of tissue types (e.g. bone, cartilage, adipose tissue); to extract the bony tissue, we selected the largest peak from the scan's histogram distribution of grayscale values, and then made small-scale adjustments to the selection range while noting the effect on the morphological accuracy of the resultant volume (i.e. whether the volume represented more or less bone than was known from dissection to be there). This 'bone selection' method resulted in more morphologically accurate volumes than an alternative method, where the grayscale thresholding range was set at the start of the MATLAB script through an iterative series of threshold steps on individual original (full grayscale range) CT slices. However, when thresholding methods were compared for the same CT datasets, analyses of cross-sectional geometry in MATLAB (see below) produced nearly identical trends, indicating the technique is robust, regardless of thresholding method.

Each resultant thresholded (i.e. 'bone-only') volume was sectioned orthogonal to the longitudinal axis of the rostrum and an image stack of cross-sections exported to the MATLAB script. The script then performed a slice-wise analysis of cross-sectional geometry, beginning by normalizing rostrocaudal positions to percentage lengths to facilitate comparison across scans (i.e. the slice containing the rostral tip represented 0% length, the slice containing the caudal end of the rostrum represented 100% length). Slices were then selected at intervals of 2% element length; this selection interval was determined via sensitivity analysis to provide a balance of resolution of data trends and script efficiency.

Table 3. Specimen information

Species	No.	LJ–FL (cm)	Mass (kg)	BL (cm)
X. gladius (SWF)	1	125	36.1	72.4
	2	138.7	38.2	77.5
	3	146.1	39.9	77.5
	4	147.3	37.7	78
M. nigricans (BM)	1	257	172.5	59.5
	2	257.8	147.1	61.7

Meristic data from both species utilized in this study: swordfish (SWF) and blue marlin (BM).
Total length estimations in billfishes are commonly measured as lower jaw–fork length (LJ–FL); bill length (BL) was measured as the distance from the tip to the naris.

For each of the 51 slices per rostrum, the script converted the grayscale 'bone-only' images to binary images (white, bone; black, soft tissue and voids) and analyzed the distribution of white pixels around the cross-section centroid in order to determine a series of variables describing rostrum cross-section geometry: second moment of area (I); cross-sectional area (A); and filled-CSA (A_f; the area of the element cross-section with any holes or internal black pixels converted to white pixels) (Fig. 9).

Second moment of area describes the distribution of material around a neutral axis (NA) in a cross-section and perpendicular to the line of applied force, and is therefore indicative of resistance to bending. Billfish rostra contain multiple tissues with different material properties, which can be accounted for by scaling the contribution of each tissue according to its Young's modulus (Gere, 2002). However, as the non-bony tissues are located closer to the NA and their moduli are as of yet unknown (although likely orders of magnitude less), we simplify the analysis by focusing only on the bone tissue and assuming it has a consistent modulus down the length of the rostrum and between species.

The second moments of area of any shape around a given axis is given by $I=\int y^2\,\mathrm{d}A$, where y is the perpendicular distance of the area element $\mathrm{d}A$ from that axis. For simple shapes, this is readily calculated analytically and tables of appropriate formula can be found in textbooks. For complex shapes, where no easy analytical equation is available, it is possible to divide the complex shape up into simple shapes for which the second moment of area is known, and add these values together weighted by the distance of the centroids of each shape to the bending axis (Gere, 2002). We apply this approach to the complex geometries of our CT data, so that for each cross section, the second moment of area about a given neutral axis (NA) is calculated with the following equation:

$$I_{\mathrm{NA}} = \sum^{n}(I_{\mathrm{pix}} + A_{\mathrm{pix}}\,y^2), \quad (1)$$

where n is the number of individual pixels; I_{pix} is the second moment of area of each pixel relative to its own centroid (a^4)/12; A_{pix} is the pixel area, a^2, where a=0.625 mm; y is the perpendicular distance from the NA (NA was determined as the axis perpendicular to the applied force passing through the centroid of each cross section). Apart from the term (I_{pix}) in the summation, this equation is identical to the standard integral; the I_{pix} term, however, is important when there are few pixels in an examined cross-section and/or y is small compared with the pixel size (i.e. at the extreme proximal or distal ends of the rostra), because the area of each pixel is proportionately more important to the cross-section second moment of area. For large and/or thick-walled cross-sections, when y is large compared with the pixel size, the corrective term I_{pix} would be negligible and our equation and the standard integral would effectively yield the same results.

However, as the second moment of area of asymmetrical sections can vary with the chosen bending axis – evidenced by the example of an architectural I-beam with a higher second moment of area when bent in line with its longer cross-sectional axis – we calculated second moment of area for bending in line with the major axis (I_{maj}) and the bending in line with the minor axis (I_{min}) of each cross-section. The major and minor axes are defined as the longest and shortest diameters of the cross-section; in both species, these structural axes correspond to the lateromedial and dorsoventral axes of the rostra, respectively (see cross-sections in Fig. 9). The ratio of the two moments ($I_{\mathrm{maj}}/I_{\mathrm{min}}$) is a mechanical aspect ratio, describing the anisotropy of bending resistance for the cross-section. Whereas an ellipse would exhibit a higher ratio, indicating a greater resistance to bending along one axis, a circle's moment ratio would be 1.0, indicating isotropy in bending resistance.

The Journal of Experimental Biology (2015) 218, 824-836 doi:10.1242/jeb.106146

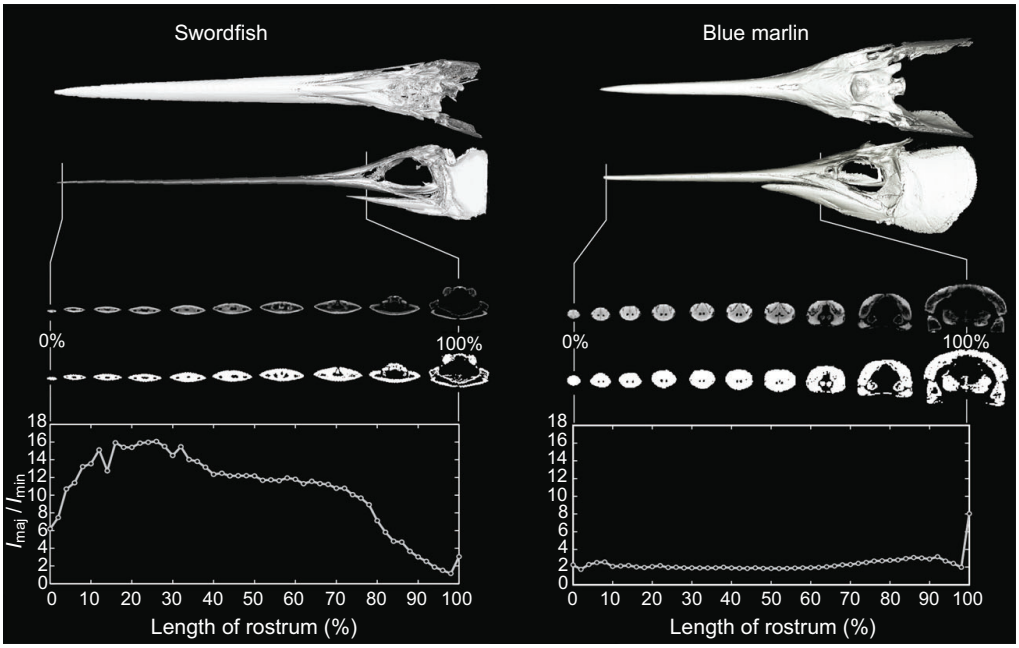

Fig. 9. Illustration of the cross-sectional shape differences between species and description of the major steps performed during the MATLAB geometric analysis. From top to bottom: complete skull renderings for both species followed by grayscale 'bone-only' thresholded rostrum sections utilized for the analysis (number of cross-sections shown has been reduced because of space contraints), followed by binary images (black and white). Binomial images were produced every 2% along the rostrum and the ratio of bending moments between two loading planes (I_{maj}/I_{min}) was calculated along the length of the rostrum.

We further described the cross-sectional distribution of material by calculating the proportion of bone (number of white pixels, A) per cross-section relative to that of the hypothetical filled cross-section (A_f):

$$\%\text{Min} = A/A_f. \quad (2)$$

In addition, the relative mineral content per cross-section was estimated by calculating the average grayscale value of mineralized tissue. As the scans were not calibrated to materials of known mineral density (e.g. using imaging phantoms of varying hydroxyapatite composition), these values are only meaningful as relative measurements and so are presented as percentages of each scan's maximum value, from 0 to 100%.

Bending experiments in a material testing system (MTS)

Billfish heads were thawed and prepared for material testing by removing all soft tissues from the skull. Once cleaned, each skull (neurocranium) was potted in fast-curing cement (Rockite, Hartline Products, Cleveland, OH, USA), firmly encasing the head while leaving the entire rostrum exposed, simulating a cantilever beam. The embedded skull was then anchored to the floor via a holding device (Fig. 10) and the tip of the rostrum fixed to the crosshead of a materials testing device by a custom-made wooden clamp that enveloped the rostrum cross section allowing vertical motion and load dispersal along the cross section. The attachment point of the MTS was located approximately 15% of the rostrum length from the tip, representing a loading point (LP) that might be expected during prey contact. To determine the reaction of tissue along the length of the rostrum to distal loads, four transverse regions were demarcated (areas 1–4, distal to proximal), starting at 30% rostrum length and spaced approximately 20% apart. The criteria for the selection of these points were based on the relative positions that represented the best locations to survey strain along the majority of the rostrum accounting for differences in length in both species. Each area was fitted with six strain gauges oriented parallel to the longitudinal axes of the rostra (C2A-13-125LW-120, Vishay Measurements Group, Inc., Raleigh, NC, USA): four on the dorsal surface (two lateral and two medial) and two on the medial ventral surface (Fig. 10). For proper strain gauge attachment, each region was smoothed with 400-grade sandpaper, and excess oil removed with acetone. Strain gauges were glued to the underlying bone with Mbond glue (Vishay Measurements Group, Inc., Raleigh, NC, USA). Because some of the skeletal elements at the base of the most proximal portion of the rostrum in blue marlin (area 4) are supported medially by soft tissue, and removing them could greatly affect the structural integrity of the rostrum, strain gauges could not be attached here, decreasing the total number of strain gauges for this species to 22.

Because the location of the NA depends on load orientation, different strain gauges were selected for the two different loading regimes utilized (lateral and dorsoventral). For example, only strain gauges located on the lateral edges of the rostrum were analyzed during lateral loading (Fig. 10). Because of the lack of knowledge of rostral bending during normal feeding behaviors in billfish and the limitations of our MTS system, displacements were fixed to ±1 cm for all bending tests. Each rostrum was loaded under displacement control at the same loading point with a 50 lb (~23 kg) load cell (JP 50, Honeywell, Golden Valley, MN, USA) at a frequency of 2 Hz in a material testing system, this was the maximum frequency allowed by our system, because higher values resulted in vibration interference (MTS System Corporation, Minneapolis, MN, USA). Loading tests were

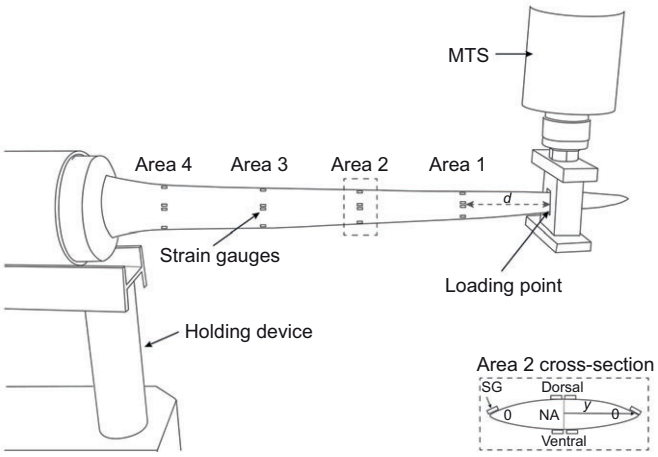

Fig. 10. Outline of the apparatus settings for the bending experiments on the material testing system (MTS) during lateral loading on a swordfish rostrum. Strain gauge (SG) location and areas along the rostrum are shown on the dorsal portion of the rostrum (from the most distal area, area 1 to the most proximal, area 4). The complete layout of strain gauges can be observed within the dashed box showing a magnified representative cross-section of area 2. Some representative examples of variables utilized for the calculation of stress are shown, where d represents the distance from the loading point to the area in question (in the figure, this is area 1) and y represents the distance from the neutral axis (NA) to one strain gauge on the dorsal surface of the cross-section. Note that although the calculation of d and y are shown here for only one strain gauge in area 1, these variables were calculated in each area (1–4).

The Journal of Experimental Biology (2015) 218, 824-836 doi:10.1242/jeb.106146

conducted in dorsoventral and lateral planes to simulate likely striking directions, with data (strains, cross-head displacement and measured force) recorded at 1000 Hz in a Megadac data collection system (Optim Electronics Corporation, Germantown, MD, USA).

Using beam theory, the following variables were estimated for each of the four areas on each rostrum. Stress was calculated using the following equation,

$$\sigma = My/I, \tag{3}$$

where M is the bending moment at each area calculated by multiplying the maximum measured load from each bending regime by the distance from the loading point to each position where most strain gauges were aligned for each area; at a given position, d, y is the in-plane distance from the NA to each strain gauge at that location (Fig. 10); and I is the second moment of area associated to each NA (mm^4). For each area's cross-section, I and y were calculated in MATLAB; for the latter, physical measurements of the distances of strain gauges from the lateral edge of the rostrum were used to determine their dorsoventral positions in each digital cross-section, and the dorsoventral distance y of those points from the neutral axis. Since we were interested in estimating the maximum stress generated by the rostrum during a set displacement, stress was calculated utilizing the largest bending moment at each area for each experiment (made by the product of the largest load and the distance from the strain gauges at each area to the loading point). Although the stress formula has been formulated based on simple structures in engineering, it has been widely used in biological systems, however, caution should be taken at interpreting its results since some deviation from its original assumptions may apply (i.e. the rostra do not have a constant cross-sectional area).

Using the stress calculated above, Young's modulus was calculated to estimate the material stiffness at each strain gauge location using the following equation:

$$E = \sigma/\varepsilon, \tag{4}$$

where ε is the strain gathered from strain gauges at the maximum bending moment. Estimating E by this method assumes that the material is linearly elastic; however, similar values of E, derived from the slope of stress-strain curves, were estimated from three-point bending experiments on the same billfish species by Atkins et al. (2014), supporting our results. Flexural stiffness ($GPa \times mm^4$) was calculated:

$$\text{Flexural stiffness} = E \times I, \tag{5}$$

where E is Young's modulus and I is the second moment of area previously calculated. This parameter estimates the resistance to bending of the rostrum at all areas, allowing an integrated understanding of material properties and responses to load along the length of the rostrum.

Biological loading scenarios: point loading and hydrodynamic loading

In addition to the geometric analyses above, we used a second MATLAB script to examine the effects of cross-sectional form on rostral stresses for both species for two possible loading conditions: point-loading (a single/point load, equivalent to the billfish striking a prey item with the tip of the rostrum) and hydrodynamic loading (a load along the full length of the rostrum, resulting from the rostrum being swiped through the water) (Fig. 11).

For each loading scenario (tip-loading vs hydrodynamic loading), stresses were calculated along the length of the rostrum for two loading directions: simulating the rostrum moving laterally (i.e. in line with the rostrum's cross-sectional major axis) and moving dorsoventrally (i.e. in line with the rostrum's cross-sectional minor axis). Stresses were calculated using equations for beam bending with the assumption of small deformations. Rostrum cross-section dimensions were determined from CT scan data (see above), with both species' rostra scaled to 700 mm tip-to-base length to allow a length-independent, interspecies comparison.

For tip-loading, we first calculated maximum normal stresses for rostrum cross-sections: since the highest stresses will be experienced on the surface of the rostrum, this can be thought of as the maximum stress experienced by a point on the surface of a cross-section that is furthest from the neutral axis in a particular loading orientation (Gere, 2002):

$$\sigma_{\text{max\_lat load}} = \frac{Fxb}{I_{\text{maj}}(x)}\,;\ \sigma_{\text{max\_DV load}} = \frac{Fxa}{I_{\text{min}}(x)}. \tag{6}$$

Maximum normal stress is a function of the applied load, F; the observed cross-section's rostrocaudal distance from the loading point (i.e. distance from the tip of the rostrum), x; a linear dimension of the cross-section in line with the applied load: b=one-half major axis length for lateral loading or a=one-half minor axis length for dorsoventral loading; and the second moment of area for that loading direction (I_{maj} or I_{min}, respectively; determined as described above and rescaled to a rostrum length of 700 mm). Maximum stresses resulting from tip-loading were calculated at 2% distance-increments from the tip to the base of the rostrum for both species and for both lateral and dorsoventral loading.

As the following calculations of hydrodynamic loading stresses are simplified considerably by using symmetrical geometric cross-sections, we selected a cross-sectional shape that could act as a proxy for actual rostral morphology, by comparing the maximum stress profiles for tip-loading for actual rostrum morphologies (see previous paragraph) with maximum stress profiles for hypothetical rostra with elliptical or diamond-shaped cross-sections. This allowed determination of the simplified cross-sectional shape that most accurately approximated stresses calculated for actual rostra, and therefore the shape which, for these purposes, was most mechanically similar to actual rostra. The aspect ratios for these idealized cross-sections were the same as those for the biological sections (i.e. the elliptical and diamond cross-sections were as wide and tall as the rostrum itself at any given tip-to-base location); these dimensions were used to calculate I along the length of the hypothetical bill using available equations for ellipses and diamonds (Gere, 2012) and these values were used in Eqn 6 to calculate maximum stresses per cross-section. The elliptical cross-section proved to be the more accurate approximation of both species' cross-sectional profiles and so was used for the subsequent hydrodynamic loading calculations.

The calculation of stresses resulting from hydrodynamic loading first required the determination of a drag coefficient, $C_D(x)$, a dimensionless number expressing the drag of a given cross-sectional shape in a moving fluid. We assumed a simple elliptical cross-section with the linear cross-sectional dimensions (i.e. major and minor axis lengths, b and a

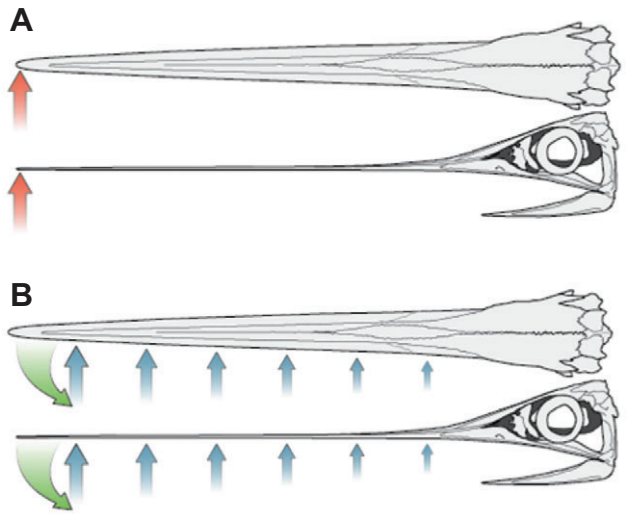

Fig. 11. Simulated point load versus hydrodynamic load scenarios in a swordfish with dorsal and lateral views of suggested loading regimes. A similar loading simulation was conducted for the blue marlin. (A) Point load simulating a lateral and dorsoventral load exerted by a prey item at the most distal portion of the rostrum (red arrow). (B) Hydrodynamic load shows the effect of water exerting a continuous load along the length of the rostrum (blue arrows) during lateral and dorsoventral movement of the head (green arrows). Dorsal view, top; lateral view, bottom.

respectively) of the actual rostrum (see previous paragraph), moving through water with subcritical Reynolds numbers (laminar flow) (Hoerner, 1965; McHenry et al., 2012). First considering movement in a direction parallel to the major axis of the cross-sections (i.e. lateral movement of the rostrum), the drag coefficient can be calculated by:

$$C_{\mathrm{D}}(x) = 0.015\,\frac{b(x)}{a(x)} + 1.1\,\frac{a(x)}{b(x)}. \quad (7)$$

Calculated drag coefficients were then used to determine the forces resulting from drag acting on each portion of the rostrum (i.e. at 2% increments down the length of the rostrum). We assumed the rostrum tip was swung through the water around the base with a velocity of 1 m s^{-1}, with the medium's density, ρ (1020 kg m^3) equivalent to 20°C seawater (Denny, 1993). The drag force per unit length for motion in the lateral direction as a function of length is:

$$D(x) = C_{\mathrm{D}}(x)\rho 2a(x)v(x)^2, \quad (8)$$

for dorsoventral motion the same equation applies, with $b(x)$ replacing $a(x)$.

The shear forces $V(x)$ in the rostrum counter-acting the drag forces imparted by the moving fluid were then calculated by integrating the drag forces along the rostrum:

$$V(x) = \int_0^x D(x)dx. \quad (9)$$

These shear forces were then integrated along the rostrum's length to determine the moments acting along the rostrum as a result of the structural response to drag forces:

$$M(x) = \int_0^x V(x)dx. \quad (10)$$

The calculated moments were then used to determine the maximum hydrodynamic loading stresses experienced by a cross-section:

$$\sigma_{\mathrm{max}}^{\mathrm{hyd}} = \frac{M(x)b}{I(x)}\,. \quad (11)$$

As with the tip-loading regime, hydrodynamic stresses were calculated at 2% increments along the bill, allowing determination of a maximum hydrodynamic stress profile for both species and in two loading directions; for dorsoventral rotation of the rostrum (i.e. motion parallel to the minor axis of the cross-sections), $a(x)$ was exchanged for $b(x)$ and vice versa in Eqns 7–11.

Acknowledgements
This study could not have been done without Anna Avrigian and Jim Frank's generous help during specimen collection. Eric Prince allowed us to collect in fishing tournaments. Rick Stanczyk, J. Gardiner, A. Ferguson, J. Morris, R. Hueter and Mote Marine laboratories provided samples. Tony Villicana and V. Melnichuk assisted during experiments. Susan Herring provided input on strain gauge selection. John Long provided feedback on backbone biomechanics. Candy Miranda performed histology work and T. Crisman and C. Mitraki provided access to microscopes. Summer Decker and J. Ford made it possible to scan specimens and render 3D images. Many thanks to M. Montocchio, R. de la Parra and E. Walker for sharing their beautiful artwork. Thank you to S. Mulvany for helping to collect specimens and editing this manuscript. Special thanks go to M. Berdugo for his continuous assistance in every step of the process. We are extremely grateful to H. Fierstine for providing insightful answers to all our questions and for his endless support and encouragement.

Competing interests
The authors declare no competing or financial interests.

Author contributions
Designed and implemented experiments: M.L.H. Designed and implemented geometrical analyses and biological loading simulations: M.N.D. and J.W.C.D. Contributed to data acquisition and analysis: M.L.H., M.N.D., D.R.H., P.J.M., J.W.C.D., G.M., M.S. and D.W. Manuscript preparation: M.L.H. Manuscript editing: P.J.M., M.N.D., D.R.H., J.W.C.D., G.M. and M.S. Figure preparation: M.L.H. and M.N.D.

Funding
This research was supported by the University of South Florida, the Guy Harvey Ocean Foundation, and the Porter Family Foundation to M.L.H. M.N.D. was supported by an Alexander von Humboldt Postdoctoral Fellowship and DFG-FR 2190/4-1 Gottfried Wilhelm Leibniz-Preis 2010.

Supplementary material
Supplementary material available online at
http://jeb.biologists.org/lookup/suppl/doi:10.1242/jeb.106146/-/DC1

References
Aleyev, Y. G. (1977). *Nekton*. The Hague: Junk.
Alfaro, M. E. (2002). Forward attack modes of aquatic feeding garter snakes. *Funct. Ecol.* **16**, 204-215.
Andrade, M. G. S., Sá, C. N., Marchionni, A. M. T., de Bittencourt, T. C. B. do. S. C. and Sadigursky, M. (2008). Effects of freezing on bone histological morphology. *Cell Tissue Bank.* **9**, 279-287.
Atkins, A., Dean, M. N., Habegger, M. L., Motta, P. J., Ofer, L., Repp, F., Shipov, A., Weiner, S., Currey, J. D. and Shahar, R. (2014). Remodeling in bone without osteocytes: billfish challenge bone structure–function paradigms. *Proc. Natl. Acad. Sci. USA* **111**, 16047-16052.
Baumiller, T. K. (1993). Crinoid stalks as cantilever beams and the nature of the stalk ligament. *Neues Jahrb. Geol. Palaeontol. Abh.* **190**, 279-297.
Biewener, A. A. and Full, R. J. (1992). *Biomechanics Structures and Systems: A Practical Approach* (ed. A. A. Biewener), Oxford: Oxford University Press.
Bonser, R. H. C (2001). The mechanical performance of medullary foam from feathers. *J. Mater. Sci. Lett.* **20**, 941-942.
Bonser, R. H. C and Purslow, P. P. (1995). The Young's Modulus of feather keratin. *J. Exp. Biol.* **198**, 1029-1033.
Cohen, L., Dean, M., Shipov, A., Atkins, A., Monsonego-Ornan, E. and Shahar, R. (2012). Comparison of structural, architectural and mechanical aspects of cellular and acellular bone in two teleost fish. *J. Exp. Biol.* **215**, 1983-1993.
Currey, J. D. (1984). *The Mechanical Adaptations of Bone*. Princeton, NJ: Princeton University Press.
Currey, J. D. (2002). *Bones: Structure and Mechanics*. Princeton, NJ: Princeton University Press.
Currey, J. (2004). Incompatible mechanical properties in compact bone. *J. Theor. Biol.* **231**, 569-580.
Davie, P. (1990). *Pacific Marlins: Anatomy and Physiology*. Palmerston North: New Zealand Massey University Press.
Denny, M. (1993). *Air and Water: The Biology and Physics of Life's Media*. Princeton, NJ: Princeton University Press.
Dill, L. M. (1974). The escape response of zebra danio (*Brachydanio rerio*). The stimulus for escape. *Anim. Behav.* **22**, 710-721.
Domenici, P., Wilson, A. D. M., Kurvers, R. H. J. M., Marras, S., Herbert-Read, J. E., Steffensen, S., Krause, S., Viblanc, P. E., Couillaud, P. and Krause, J. (2014). How sailfish use their bills to capture schooling prey. *Proc. R. Soc. B Biol. Sci.* **281**, 20140444.
Ennos, A. R. (1993). The mechanics of the flower stem of the sedge *Carex acutiformis*. *Ann. Bot.* **72**, 123-127.
Etnier, S. A. (2003). Twisting and bending of biological beams: distribution of biological beams in a stiffness mechanospace. *Biol. Bull.* **205**, 36-46.
Etnier, S. A. and Vogel, S. (2000). Reorientation of daffodil (*Narcissus*: Amaryllidaceae) flowers in wind: drag reduction and torsional flexibility. *Am. J. Bot.* **87**, 29-32.
Field, D. J., Lin, S. C., Ben-Zvi, M., Goldbogen, J. A. and Shadwick, R. E. (2011). Convergent evolution driven by similar feeding mechanics in balaenopterid whales and pelicans. *Anat. Rec.* **294**, 1273-1282.
Fierstine, H. L. (1974). The paleontology of billfish-the state of the art. In *Part 2. Review and contributed papers*. Proc. Int. Billfish Symposium, Kailua-Kona, Hawaii, August 9–12, 1972. pp. 34–44.
Fierstine, H. L. (1990). A paleontological review of three billfish families (Istiophoridae, Xiphiidae and Xiphiorhynchidae). In *Planning the future of billfishes. Part 2. Contributed papers* (ed. R. H. Stroud). Proc. 2nd Int. Billfish Symposium, Kailua-Kona, Hawaii, August 1–5, 1988. pp. 11-19.
Fierstine, H. L. (1997). An Atlantic Blue Marlin, *Makaira nigricans*, impaled by two species of billfishes (Teleostei: Istiophoridae). *Bull. Mar. Sci.* **61**, 495-499.
Fierstine, H. L. (2006). Fossil history of billfishes (Xiphioidei). *Bull. Mar. Sci.* **79**, 433-453.
Fierstine, H. L. and Crimmen, O. (1996). Two erroneous, commonly cited examples of "swordfish" piercing wooden ships. *Copeia* **1996**, 472-475.
Fierstine, H. L. and Voigt, N. L. (1996). Use of rostral characters for identifying adult billfishes (Teleostei: Perciformes: Istiophoridae and Xiphiidae). *Copeia* **1996**, 148-161.

Fierstine, H. L., Cailliet, G. M. and Neer, J. A. (1997). Shortfin Mako, *Isurus oxyrinchus*, impaled by blue marlin, *Makaira nigricans* (Teleostei: Istiophoridae). *Bull. South. Calif. Acad. Sci.* **3**, 117-121.
Frazier, J. G., Fierstine, H. L., Beavers, S. C., Achaval, F., Suganuma, H., Pitman, R. L., Yamaguchi, Y. and Prigioni, C. M. (1994). Impalement of marine turtles (Reptitia, Chelonia: Cheloniidae and Dermochelyidae) by billfishes (Osteichthyes, Perciformes: Istiophoridae and Xiphiidae). *Env. Biol. Fish.* **39**, 85-96.
Gere, J. M. (2002). *Mechanics of Materials*, 5th edn. Stamford, CT: Brooks/Cole Publishing Co.
Goode, G. B. (1883). Material for a history of the swordfish. *Rept. U.S. Fish. Comm.* **8**, 289-386.
Gregory, W. K. and Conrad, G. M. (1937). The comparative osteology of the swordfish (*Xiphias*) and the sailfish (*Istiophorus*). *Am. Mus. Novitates* **952**, 7-25.
Gudger, E. W. (1940). The allegated pugnacity of the swordfish and the spearfishes as shown by their attacks on vessels. *R. Asiatic. Soc. Bengal Branch Mem.* **2**, 215-231.
Habegger, M. L., Motta, P. J., Huber, D. R. and Dean, M. N. (2012). Feeding biomechanics and theoretical calculations of bite force in bull sharks (*Carcharhinus leucas*) during ontogeny. *Zoology* **115**, 354-364.
Hebrank, J. H., Hebrank, M. R., Long, J. H., Jr, Block, B. A. and Wainwright, S. A. (1990). Backbone mechanics of the blue marlin *Makaira nigricans* (Pisces, Istiophoridae). *J. Exp. Biol.* **148**, 449-459.
Hoerner, S. F. (1965). *Fluid-Dynamic Drag*. Brick Town, NJ: Hoerner Fluid Dynamics.
Horton, J. M. and Summers, A. P. (2009). The material properties of acellular bone in a teleost fish. *J. Exp. Biol.* **212**, 1413-1420.
Huber, D. R., Neveu, D. E., Stinson, C. M., Anderson, P. A. and Berzins, I. K. (2013). Mechanical properties of sand tiger shark (*Carcharias taurus*) vertebrae in relation to spinal deformity. *J. Exp. Biol.* **216**, 4256-4263.
Kemp, T. J., Bachus, K. N., Nairn, J. A. and Carrier, D. R. (2005). Functional tradeoffs in the limb bones of dogs selected for running versus fighting. *J. Exp. Biol.* **208**, 3475-3482.
Koehl, M. A. R. (1976). Mechanical design in sea anemones. In *Coelenterate Ecology and Behavior* (ed. G.O. Mackie), pp. 23-31. New York, NY: Plenum Publishing Corp.
Koehl, M. A. R. (1977). Mechanical organization of cantilever like sessile organism: sea anemonies. *J. Exp. Biol.* **6**, 127-142.
Krauss, S., Monsonego-Ornan, E., Zelzer, E., Fratzl, P. and Shahar, R. (2009). Biological materials: mechanical function of a complex three-dimensional suture joining the bony elements in the shell of the redeared slider turtle. *Adv. Mater.* **21**, 407-412.
Ma, J.-f., Chen, W.-y., Zhao, L. and Zhao, D.-h. (2008). Elastic buckling of bionic cylindrical shells based on bamboo. *J. Bion. Eng.* **5**, 231-238.
Macesic, L. J. and Summers, A. P. (2012). Flexural stiffness and composition of the batoid propterygium as predictors of punting ability. *J. Exp. Biol.* **215**, 2003-2012.
Macleod, G. D. (1980). Mechanical properties of contour feathers. *J. Exp. Biol.* **87**, 65-71.
Magwene, P. M. and Socha, J. J. (2013). Biomechanics of turtle shells: how whole shells fail in compression. *J. Exp. Zool.* **319**, 86-98.
Markey, M. J., Main, R. P. and Marshall, C. R. (2006). In vivo cranial suture function and suture morphology in the extant fish *Polypterus*: implications for inferring skull function in living and fossil fish. *J. Exp. Biol.* **209**, 2085-2102.
McGowan, C. (1988). Differential development of the rostrum and mandible of the swordfish (*Xiphias gladius*) during ontogeny and its possible functional significance. *Can. J. Zool.* **66**, 496-503.
McHenry, C. R., Clausen, P. D., Daniel, W. J. T., Meers, M. B. and Pendharkar, A. (2006). The biomechanics of the rostrum in crocodilians: a comparative analysis using finite-element modeling. *Anat. Rec.* **288A**, 827-849.
McHenry, M. J., Claverie, T., Rosario, M. V. and Patek, S. N. (2012). Gearing for speed slows the predatory strike of a mantis shrimp. *J. Exp. Biol.* **215**, 1231-1245.
Meyers, M. A., McKittrick, J. and Chen, P.-Y. (2013). Structural biological materials: critical mechanics-materials connections. *Science* **339**, 773-779.
Miserez, A., Schneberk, T., Sun, C., Zok, F. W. and Waite, J. H. (2008). The transition from stiff to compliant materials in squid beaks. *Science* **319**, 1816-1819.
Nakamura, I. (1983). Systematics of the billfishes (Xiphiidae and Istiophoridae). *Publ. Seto. Mar. Biol. Lab.* **28**, 255-396.
Nakamura, I. (1985). *Billfishes of the world*. FAO Species Catalogue. FAO Fish. Synop. No.125, vol. 5, 1–65.
Nohara, K., Hiroshi, O., Motoki, N., Kazuhiko, H., Nobuaki, S., Makoto, O. and Chow, S. (2003). Biological investigation on two types of bill internal structure of swordfish (*Xiphias gladius*) and genetic differentiation between the North and South Atlantic stocks. *Bull. Fish. Res. Agen.* **7**, 1-13.
Opperman, L. A. (2000). Cranial sutures as intramembranous bone growth sites. *Dev. Dyn.* **219**, 472-485.
Ovchinnikov, V. V. (1970). *Swordfish and billfishes in the Atlantic Ocean. Ecology and functional morphology*. Isr. Prog. Sci. Trans. NOAA NMFS TT 71–50011.
Politi, Y., Priewasser, M., Pippel, E., Zaslansky, P., Hartmann, J., Siegel, S., Li, C., Barth, F. G. and Fratzl, P. (2012). A spider's fang: how to design an injection needle using chitin-based composite material. *Adv. Funct. Mat.* **22**, 2519-2528.
Poplin, C., Poplin, F. and Rieqles, A. (1976). Quelques particularités anatomiques et histologiques du rostre de l'espadon *(Xiphias gladius* L.). *C. R. Acad. Sci. Ser. D.* **282**, 1105-1108.
Rafferty, K. L., Herring, S. W. and Marshall, C. D. (2003). Biomechanics of the rostrum and the role of facial sutures. *J. Morph.* **44**, 257–233.
Sagong, W., Jeon, W.-P. and Choi, H. (2013). Hydrodynamic characteristics of the sailfish (*Istiophorus platypterus*) and swordfish (*Xiphias gladius*) in gliding postures at their cruise speeds. *PLoS ONE* **8**, e81323.
Scott, W. B. and Tibbo, S. N. (1968). Food and feeding habits of swordfish, *Xiphias gladius*, in the Western North Atlantic. *J. Fish. Res. Bd. Canada* **25**, 903-919.
Seki, Y., Schneider, M. S. and Meyers, M. A. (2005). Structure and mechanical behavior of a toucan beak. *Acta Mat.* **53**, 5281-5296.
Shimose, T., Yokawa, K., Saito, M. and Tachihara, K. (2007). Evidence for use of the bill by blue marlin, *Makaira nigricans*, during feeding. *Ichtyol. Res.* **54**, 420-422.
Stillwell, C. E. and Kohler, N. E. (1985). Food and feeding ecology of the swordfish *Xiphias gladius* in the western North Atlantic Ocean with estimates of daily ration. *Mar. Ecol.* **22**, 239-247.
Sun, Z., Lee, E. and Herring, S. W. (2004). Cranial sutures and bones: growth and fusion in relation to masticatory strain. *Anat. Rec. Part A* **276A**, 150-161.
Talbot, F. H. and Penrith, J. J. (1964). Spearing behavior in feeding in the black marlin, *Istioampax marlina*. *Copeia* **1964**, 468.
Taylor, J. R. A., Hebrank, J. and Kier, W. M. (2007). Mechanical properties of the rigid and hydrostatic skeletons of molting blue crabs, *Callinectes sapidus* Rathbun.. *J. Exp. Biol.* **210**, 4272-4278.
Visser, A. W. (2001). Hydromechanical signals in the plankton. *Mar. Ecol. Prog. Ser.* **222**, 1-24.
Vogel, S. (2003). *Comparative Biomechanics: Life's Physical World*. Princeton: Princeton University Press.
Wainwright, S. A., Biggs, W. D., Currey, J. D. and Gosline, J. M. (1976). *Mechanical Design in Organisms*. Princeton, NJ: Princeton University Press.
Wisner, R. (1958). Is the spear of istiophorid fishes used in feeding? *Pac. Sci.* **12**, 60-70.
Wroe, S., Huber, D. R., Lowry, M., McHenry, C., Moreno, K., Clausen, P., Ferrara, T., Cunningham, E., Dean, M. N. and Summers, A. P. (2008). Three-dimensional computer analysis of white shark jaw mechanics: how hard can a great white bite? *J. Zool.* **276**, 336-342.